A particle accelerated CFD-BEM technique applied to aeroacoustic scattering

P. Croaker[1], N. Kessissoglou[1] and S. Marburg[2]

[1] School of Mechanical & Manufacturing Engineering, UNSW Australia, Sydney, NSW 2052, Australia

[2] LRT4 – Institute of Mechanics, Universität der Bundeswehr München, D-85579 Neubiberg, Germany

ABSTRACT

A particle accelerated computational fluid dynamics (CFD) - boundary element method (BEM) technique is proposed that allows the total sound pressure field produced by low Mach number flow past a rigid body to be predicted. An incompressible CFD solver is used to calculate the transient hydrodynamic flow field. The CFD/BEM coupling technique is then used to compute the acoustic pressure and pressure gradient incident on the body. The incident acoustic field is calculated based on a near-field solution of Lighthill's analogy. Numerical techniques are employed to accurately evaluate the strongly singular and hypersingular surface and volume integrals. A particle condensation technique is applied to accelerate the incident field computations and reduce the amount of data that must be stored during the CFD analysis. The incident field is then combined with a BEM model of the body to predict the scattered sound pressure field. The BEM model solves the Burton-Miller boundary integral equations to guarantee a unique solution at all frequencies. Results from the particle accelerated CFD-BEM technique are presented for flow past a circular cylinder with Reynolds number, Re_D=100 and Mach number, M=0.02. The directivity of the sound pressure field at the vortex shedding frequency and its harmonics predicted using the condensation technique are compared with non-condensed results as well as results obtained using Curle's analogy.

Keywords: Computational fluid dynamics, flow induced noise, boundary element method
I-INCE Classification of Subjects Number(s): 21.6.5

1. INTRODUCTION

Lighthill (1, 2) reformulated the Navier-Stokes equation into a wave equation to represent acoustic sources generated by fluid motion and the propagation of these acoustic sources. He derived an acoustic analogy that demonstrates sound generated by a turbulent fluid flow is equivalent to the sound generated by a distribution of acoustic quadrupoles computed from the instantaneous velocity fluctuations. The acoustic sources are extracted from the transient flow field data and then a wave equation, derived from Lighthill's acoustic analogy, is solved to predict the propagation of these acoustic sources. Curle (3) extended Lighthill's analogy to include the effect of stationary boundaries present in the turbulent flow on the sound generation. The contribution of a stationary rigid body on the sound generated by unsteady flow was shown to be equivalent to a surface distribution of acoustic dipoles computed from the instantaneous pressure fluctuations on the body. Gloerfelt et al. (4) showed that the surface distribution of dipoles from Curle's analogy represent the scattered field produced when sound waves travelling from the flow noise sources reach the surface of the stationary rigid body.

For low Mach number flows past an acoustically compact body, flow field data obtained from either a compressible or an incompressible CFD analysis will produce accurate acoustic results when used in conjunction with Curle's analogy. However, if the body is not acoustically compact, Curle's analogy does not accurately predict the scattered sound field unless the compressibility of the fluid is included in the hydrodynamic analysis (5, 6). However, for low Mach number flow induced noise simulations, it is incredibly challenging and computationally expensive to include the fluid compressibility in the hydrodynamic analysis (7). Schram (5) derived a boundary element method (BEM) extension of Curle's analogy for non-compact bodies at low Mach numbers. The pressure was decomposed into acoustic and hydrodynamic components. A boundary integral equation was then developed by splitting the volume sources into near-field and far-field regions. In contrast, Khalighi et al. (6) solved a boundary integral equation developed from Lighthill's wave equation using BEM. In their work, the volume distribution of quadrupole sources in the flow field act as the acoustic sources and no assumptions about the compactness of the source region is made. The approach of Khalighi et al. (6) is an excellent method for predicting low Mach number flow induced noise in the presence of both acoustically compact or non-compact bodies. One drawback however is that the propagation of the acoustic waves produced by the hydrodynamic noise sources to the body were incorporated directly in the authors's own BEM solver, which relies on the CHIEF method (8) to deal with the irregular frequencies that are encountered in exterior BEM problems. Marburg and Amini (9) show that the Burton and Miller method (10) is a more reliable and robust method to remove the irregular frequencies compared to the CHIEF method. The Burton and Miller method involves a linear combination of the surface Helmholtz equation and its differentiated form and provides a unique solution for exterior acoustic problems at all frequencies (9).

In this paper, a particle accelerated hybrid CFD-BEM technique is developed to predict low Mach number flow induced noise and the resulting radiated sound pressure generated by a body immersed in the flow. A near-field formulation for the acoustic pressure and pressure gradient based on Lighthill's acoustic analogy is derived. This near-field formulation calculates the propagation of acoustic waves from the flow noise sources to the body surface. A particle condensation technique to reduce the amount of data that must be stored using the CFD analysis and accelerate the computations of the incident field on the body is employed. The near-field formulation is applied to the acoustic sources immediately adjacent to the body to ensure the singularities present in the harmonic Green's function and its derivatives are regularised in a mathematically robust manner. The propagation of the acoustic waves from sources further away from the body are calculated using the particle condensation technique. The accuracy and low computational cost of this particle accelerated hybrid CFD-BEM technique is demonstrated by calculating the incident acoustic field on a cylinder in cross flow at a Reynolds number of Re_D=100 and Mach number of M=0.02. The incident acoustic field is then applied to a BEM solver based on the Burton and Miller formulation to predict the radiated sound pressure scattered by the body.

2. NUMERICAL METHODS

2.1 Transient Laminar CFD Simulation

To demonstrate the particle accelerated CFD-BEM technique, laminar vortex shedding from a cylinder of diameter D is simulated at a Reynolds number $Re_D = 100$ and Mach number $M = 0.02$. At this Reynolds number the flow is in the laminar unsteady regime and is predominantly two-dimensional, with negligible spanwise contribution (11). Hence, only a two-dimensional CFD simulation is considered here. A two-dimensional circular domain around the cylinder has been modelled and analysed using ESI Group's CFD-ACE+ software package. The velocity-pressure form of the incompressible Navier-Stokes equations are solved by CFD-ACE+ in this instance. The incompressible Navier-Stokes equations are given by:

$$\begin{aligned}
\rho_0 \frac{\partial (u_x)}{\partial t} + \rho_0 \nabla \cdot (\mathbf{u} u_x) &= -\frac{\partial p}{\partial x} + \nabla \cdot (\mu \nabla u_x) \\
\rho_0 \frac{\partial (u_y)}{\partial t} + \rho_0 \nabla \cdot (\mathbf{u} u_y) &= -\frac{\partial p}{\partial y} + \nabla \cdot (\mu \nabla u_y) \\
\rho_0 \frac{\partial (\rho u_z)}{\partial t} + \rho_0 \nabla \cdot (\mathbf{u} u_z) &= -\frac{\partial p}{\partial z} + \nabla \cdot (\mu \nabla u_z) \\
\nabla \cdot \mathbf{u} &= 0
\end{aligned} \tag{1}$$

where $\mathbf{u} = (u_x, u_y, u_z)$ is the velocity vector. CFD-ACE+ uses an iterative, segregated solution method with the pressure-velocity coupling handled using the SIMPLEC algorithm.

The model used for the CFD simulation is shown in Figure 1, with the mesh topology in the vicinity of the cylinder inset. The interior of the computational domain extends radially for $25D$. A sponge layer extends radially for an additional $20D$. The interior domain contains 71,760 quadrilateral cells, with a cell spacing adjacent to the cylinder of $0.005D$. The cell distribution is biased so that the wake region contains a high cell density to resolve the vortices shed from the cylinder. The sponge layer contains an additional 6,960 quadrilateral cells. The cell size on either side of the interface between the interior domain and sponge layer is uniform, with the cells in the sponge layer then growing rapidly in the radial direction.

The viscosity in the sponge layer has been artificially increased by a factor of 35 to damp out the fluctuations in the velocity field in an attempt to force the acoustic source terms to zero at the boundary. A steady state simulation was performed with the converged solution used as the initial condition of the transient simulation. The simulations were second order accurate in time and space, with a central difference scheme used for the spatial discretisation and a Crank-Nicholson scheme used for the temporal discretisation. The transient

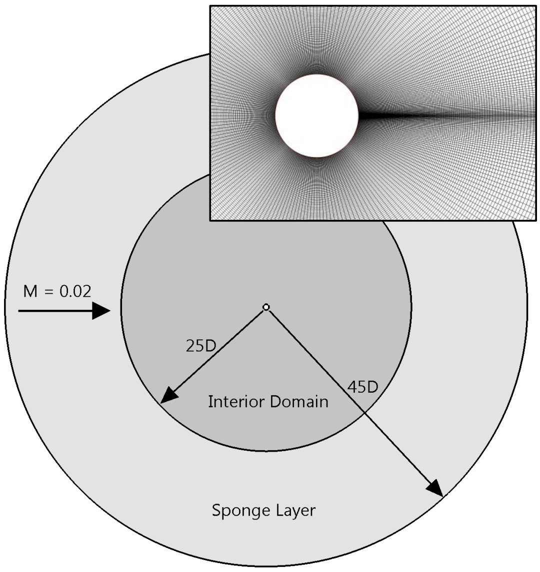

Figure 1 – Domain shape and size for CFD analysis

simulation was executed with a non-dimensionalised time step size of $\triangle t\frac{U_\infty}{D} = 2.99\mathrm{E}-3$, where U_∞ is the free stream velocity. This corresponds to a Courant-Fredrichs-Lewy (CFL) number of approximately 0.6. The simulation was allowed to progress until the flow field achieved periodicity. After this periodicity had been attained, recording of the acoustic source data commenced and data from eight vortex shedding periods was obtained.

2.2 Incident Field from Lighthill's Acoustic Analogy

The authors have derived formulations for the near-field pressure and pressure gradient based on Lighthill's acoustic analogy (12). In this work, these formulations are extended to include the surface integrals arising when the Lighthill tensor is non-zero on the boundary. Such a situation arises if viscous effects are important, or for cases when the boundary is not stationary. Here, the former situation is considered. The formulations for the near-field pressure and pressure gradient including the surface integrals are given by

$$\begin{aligned} p_a(\mathbf{x},\omega) = \lim_{\varepsilon\to 0}\Bigg\{ &\int_{(\Omega-V_\varepsilon)} \hat{T}_{ij}(\mathbf{y},\omega)\, G_{h_{ij}} d\mathbf{y} \\ &+ \int_{(\Gamma-\Gamma_\varepsilon)} \left[G_h \frac{\partial \hat{T}_{ij}(\mathbf{y},\omega)}{\partial y_i}\cdot n_j - \hat{T}_{ij}(\mathbf{y},\omega)\, G_{h_j}\cdot n_i \right] d\mathbf{y} \Bigg\} \\ &- \hat{T}_{ij}(\mathbf{x},\omega)\, c_{ij}(\mathbf{x}) \end{aligned} \tag{2}$$

$$\begin{aligned} q_{a,k}(\mathbf{x},\omega) = \lim_{\varepsilon\to 0}\Bigg\{ &\int_{(\Omega-V_\varepsilon)} \hat{T}_{ij}(\mathbf{y},\omega)\, G_{h_{ijk}} d\mathbf{y} - \hat{T}_{ij}(\mathbf{x},\omega)\frac{e_{ijk}(\mathbf{x})}{\varepsilon} \\ &+ \int_{(\Gamma-\Gamma_\varepsilon)} \left[G_{h_k} \frac{\partial \hat{T}_{ij}(\mathbf{y},\omega)}{\partial y_i}\cdot n_j - \hat{T}_{ij}(\mathbf{y},\omega)\, G_{h_{jk}}\cdot n_i \right] d\mathbf{y} \Bigg\} \\ &+ \frac{\partial \hat{T}_{ij}(\mathbf{x},\omega)}{\partial y_i} d_{jk}(\mathbf{x}) - \frac{\partial \hat{T}_{ij}(\mathbf{x},\omega)}{\partial y_l} f_{ijkl}(\mathbf{x}) \end{aligned} \tag{3}$$

where p_a is the near-field pressure and $q_{a,k}$ is the pressure gradient in the k^{th} direction. y_i is the i^{th} component of the acoustic source point position vector $\mathbf{y}$. $\mathbf{x}$ is the field point where the near-field pressure and pressure gradient are recovered. Ω and Γ are respectively the computational domain and its boundary. V_ε and Γ_ε respectively represent an exclusion neighbourhood and its intersection with the boundary Γ. This exclusion neighbourhood allows the singularities occuring when $\mathbf{x} = \mathbf{y}$ to be regularised. n_j is the j^{th} component of the normal vector pointing out of the fluid on $(\Gamma - \Gamma_\varepsilon)$. c_{ij}, d_{jk}, e_{ijk} and f_{ijkl}, are free-term coefficients arising from evaluation of the surface integrals on the boundary of the exclusion neighbourhood V_ε. The harmonic free field Green's function of the wave equation is given by

$$G_h = \frac{e^{\tilde{i}k_a r}}{4\pi r} \tag{4}$$

where $\tilde{i}$ is the imaginary unit, k_a is the acoustic wavenumber and $r = |\mathbf{x} - \mathbf{y}|$. The derivative of the Green's function in the y_i direction is represented by G_{h_i}, with repeated indices indicating higher order differentiation. T_{ij} is the Lighthill tensor and is given by

$$T_{ij} = \rho_f u_i u_j + \left(p_h - c_0^2 \rho_f\right) \delta_{ij} - \tau_{ij} \tag{5}$$

where ρ_f is the fluid density, p_h is the hydrostatic pressure, u_i, u_j are respectively the i^{th} and j^{th} components of the velocity vector, δ_{ij} is the Kronecker delta and τ_{ij} is the viscous stress tensor. The first term on the right hand side of equation (5) represents the contribution due to the Reynolds stresses. The second term relates to sound generation by non-isotropic processes and the third term represents the contributions due to viscous stresses. In the derivation of equations (2) and (3) a harmonic time dependence of $e^{-i\omega t}$ has been assumed and all solution variables represent Fourier transformed quantities. Additional details of the formulations for near-field pressure and pressure gradient as well as their numerical treatment can be found in Ref (12).

2.3 Particle Condensation Technique

A particle condensation technique previously developed by the authors (13) is used to spatially condense the acoustic source data and thereby accelerate the calculation of the incident pressure and pressure gradient generated by the volumetric flow noise sources. The method uses a particle approximation of the acoustic source distribution and employs a Taylor series expansion of the harmonic Green's function to spatially condense the underlying acoustic sources and preserve their multipole moments. The method is termed an m-Multipole Particle Condensation method and is given the abreviation mMPC, where m denotes the order of terms retained from the Taylor series expansion. Also, m corresponds to the order of the moments stored for the underlying acoustic source data. For example, if only the zeroth moments of the underyling acoustic sources are retained in the particle approximation, the method is given the abbreviation 0MPC. If zeroth, first, and second moments of the underlying acoustic sources are used, the method is termed 2MPC. Additional details of the mMPC technique are available in Ref. (13).

2.4 Coupling the Near-Field Formulation and Particle Condensation Technique

To calculate the incident acoustic field on the rigid cylinder, the domain is split into two regions. The inner region, which contains the body, is solved using the formulations for the near-field pressure and pressure gradient given by equations (2) and (3), respectively. The outer region is solved using the particle condensation technique for the acoustic pressure and pressure gradient. Using this approach, the near-field effects are accurately resolved and further away from the body, the acoustic sources are spatially condensed to reduce the amount of data that must be stored and to accelerate the acoustic propagation calculations.

The domain splitting is achieved using two spatial window functions. A spatial window function $\psi_{mMPC}(|\mathbf{y}|)$ was introduced in the derivation of the mMPC technique to force the acoustic sources to zero on the external boundary of the domain. This window function is modified here for use near a body immersed in the flow. In addition, a spatial window function $\psi_{nf}(|\mathbf{y}|)$ is applied to the acoustic source distribution for the near-field formulation. Figure 2 shows a simple schematic diagram which demonstrates these two spatial window functions in one dimension.

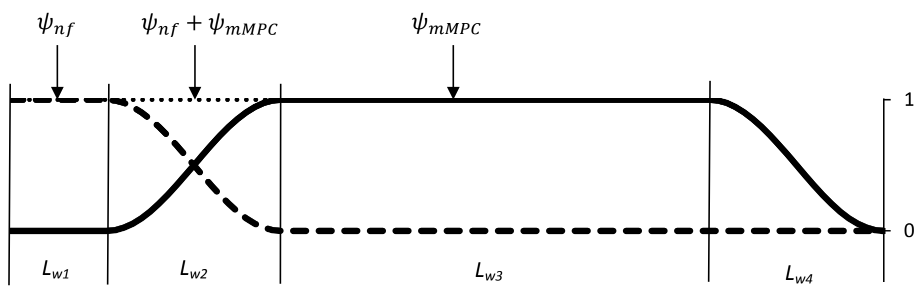

Figure 2 – Schematic diagram demonstrating the spatial window functions $\psi_{mMPC}(|\mathbf{y}|)$ and $\psi_{nf}(|\mathbf{y}|)$

In Figure 2 the surface of the cylinder is at the left hand edge. L_{w1} is the distance from the body where only near-field formulations for the pressure and pressure gradient are solved, with the near-field window function

$\psi_{nf}(|\mathbf{y}|) = 1$ and the particle window function $\psi_{mMPC}(|\mathbf{y}|) = 0$. L_{w2} represents the distance over which the near-field window function gradually decreases from 1 to 0 and the particle window function gradually increases from 0 to 1. Within this region, sources contribute to the incident field predicted by both the near-field formulation and the particle condensation technique. It is important to ensure that $\psi_{nf}(|\mathbf{y}|) + \psi_{mMPC}(|\mathbf{y}|) = 1$ so that the source distribution is conserved. L_{w3} represents the distance for which the particle window function is unity ($\psi_{mMPC}(|\mathbf{y}|) = 1$), where the acoustic sources are fully condensed. The particle window function then decreases gradually over the distance L_{w4} to a value of zero at the source truncation boundary. The following expressions are used to describe the near-field and particle spatial window functions

$$\psi_{nf}(|\mathbf{y}|) = \begin{cases} 1 & 0 \le |\mathbf{y}_b| \le L_{w1} \\ 0.5\left(1+\cos\left(\frac{\pi(|\mathbf{y}_b|-L_{w1})}{L_{w2}-L_{w1}}\right)\right) & L_{w1} < |\mathbf{y}_b| \le L_{w1}+L_{w2} \\ 0 & |\mathbf{y}_b| > L_{w1}+L_{w2} \end{cases} \tag{6}$$

$$\psi_{mMPC}(|\mathbf{y}|) = \begin{cases} 0 & 0 \le |\mathbf{y}_b| \le L_{w1} \\ 0.5\left(1-\cos\left(\frac{\pi(|\mathbf{y}_b|-L_{w1})}{L_{w2}-L_{w1}}\right)\right) & L_{w1} < |\mathbf{y}_b| \le L_{w1}+L_{w2} \\ 1 & L_{w1}+L_{w2} < |\mathbf{y}_b| \le L_{w1}+L_{w2}+L_{w3} \\ 0.5\left(1+\cos\left(\frac{\pi(|\mathbf{y}_b|-L_{w3})}{L_{w4}-L_{w3}}\right)\right) & L_{w1}+L_{w2}+L_{w3} < |\mathbf{y}_b| \le L_{w1}+L_{w2}+L_{w3}+L_{w4} \end{cases} \tag{7}$$

where $|\mathbf{y}_b|$ represents the normal distance from the source point to the body.

2.5 Particle Condensation Technique for Incident Field Prediction

Non-condensed data is required for all acoustic sources within $\mathbf{y}_b \le L_{w1} + L_{w2}$ of the body. From an efficiency and storage point of view, the window dimensions L_{w1} and L_{w2} should be as small as possible to reduce the overall data storage commitment and accelerate the acoustic propagation analyses. The particles are placed on concentric circles of increasing radius with the innermost concentric ring of particles placed at a distance L_{w1} from the cylinder surface. The particle distribution is determined based on the following procedure.

1. The first particle on each circle is placed where the positive x axis intersects the circle.
2. The remaining particles are evenly distributed around the circumference of circle g with particle separation d_g.
3. The circle radius is increased by $d_g a$ where the parameter a controls the growth of the particle distribution. The new particle separation for circle $g+1$ is approximated by $d_{g+1} = d_g a$.
4. The number of particles around circle $g+1$ is then obtained.

The previous procedure is repeated until the circle radius exceeds the bounds of the analysis domain corresponding to $45D$, where D is the diameter of the cylinder. The particle distribution used in the present work is obtained by setting $a = 1.1$ and placing 44 particles on the inner circle. This produces a particle separation on the innermost ring of particles of $d_1 = \frac{\pi}{22}$ for window parameters $L_{w1} = 1.44d_1$ and $L_{w2} = 3.96d_1$.

2.6 Incident and Scattered Acoustic Fields

The two-dimensional BEM model consisted of 180 linear one-dimensional elements around the circumference of the cylinder, with the vertices placed on the cylinder in 2° increments with 0° aligned with the direction of fluid flow. The vertices of these BEM elements also represent the field points used to calculate the incident acoustic field. The AEBEM2 subroutine of Kirkup (14) was used to solve the Burton and Miller formulation for acoustic scattering. The particle accelerated hybrid CFD-BEM technique here has been developed for three-dimensional applications and hence the acoustic propagation was carried out in three dimensions. An artificial thickness of $0.1D$ was assigned to the two-dimensional CFD cells and 100 identical copies of these sources were extruded out of the plane of the flow. Symmetry about the plane of the flow was taken into account, resulting in a source region with an out-of-plane span of $20D$. Beyond $20D$ the incident pressure and pressure gradient was insensitive to further increases in the out-of-plane span. The field points were placed on a circle of radius $6000D$ centred on the cylinder in 2° increments with 0° aligned with the direction of fluid flow. The direct radiation from the volume quadrupole sources to the far field was not considered here. Only the scattered acoustic pressure is recorded at the far-field locations.

3. RESULTS AND DISCUSSION

3.1 Hydrodynamic Analysis

The hydrodynamic analysis has been presented previously by the authors (13) and is briefly summarised here. Figure 3 shows a plot of the vorticity in the flow field at one instance in time, with the first black arc representing the boundary of the sponge layer. The vorticity generated at the cylinder surface is shed from the cylinder and travels downstream as vortex pairs. Figure 3 shows that the sponge layer is effective in damping out the vorticity before reaching the downstream boundary. Figure 4 shows the frequency spectra of the fluctuating lift and drag forces exerted on the cylinder. The fundamental vortex shedding frequency occurs at Strouhal number $S_t = 0.165$. This figure also illustrates that peaks of the fluctuating lift force occur at odd harmonics of the vortex shedding frequency and peaks of the drag force occur at even harmonics.

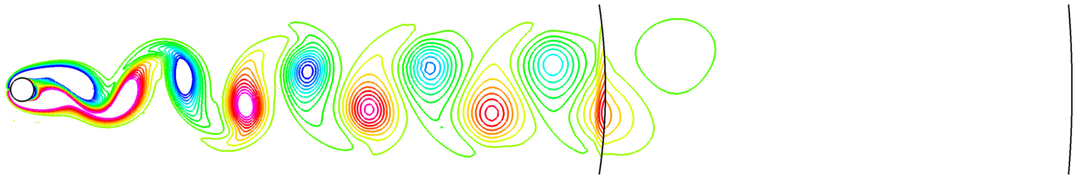

Figure 3 – Vorticies in wake of cylinder. Dimensionless vorticity γ contours from $\gamma_{min} = -1$ to $\gamma_{max} = 1$ with an increment of 0.1

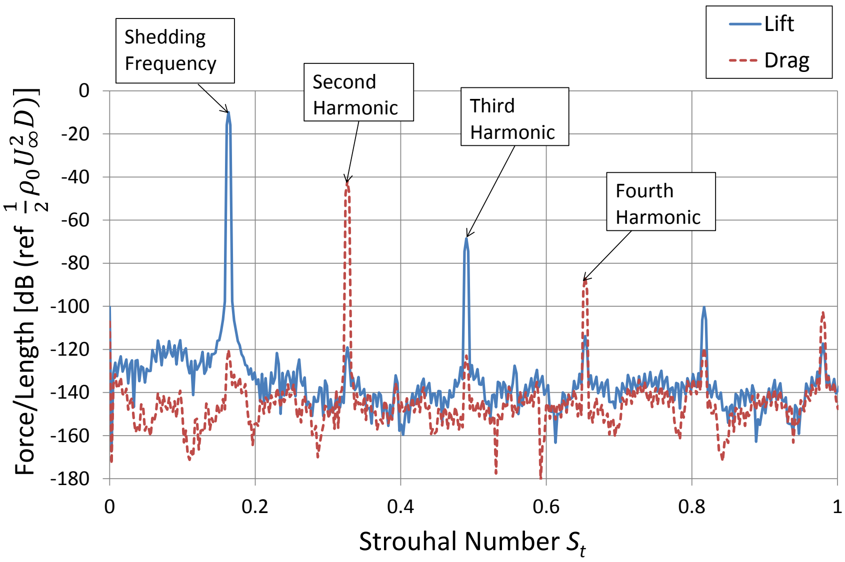

Figure 4 – Frequency spectra of the lift and drag forces

Table 1 compares the results obtained with the present hydrodynamic simulation with reference solutions from literature. A more detailed discussion of these results can be found in Ref. (13). Table 1 shows a comparison of the Strouhal number, time averaged drag coefficient $\bar{C_D}$, peak-to-peak lift coefficient $\triangle C_L$ and time averaged base-pressure coefficient $-\bar{C_{Pb}}$. The reference values are taken from the experimental results of Fey (15), empirical expressions derived by Norberg (16) and the numerical simulations of Posdziech and Grundmann (17) and Martìnez-Lera and Schram (11). The results from the present method is in excellent agreement with the data from literature.

Table 1 – Comparison of the hydrodynamic results with reference values

	S_t	$\bar{C_D}$	$\triangle C_L$	$-\bar{C_{Pb}}$
Refs. (15, 16)	0.164 Ref. (15)	–	0.643 Ref.(16)	–
Ref. (17)	0.165	1.331	0.647	0.717
Ref. (11)	0.170	1.393	0.686	0.787
Present	0.165	1.326	0.640	0.698

3.2 Scattered Field

3.2.1 Near-field formulation only

Figure 5 presents the directivity of the acoustic pressure at the first four harmonics of the vortex shedding frequency at $r = 6000D$. The incident field was computed using only the near-field formulations for the pressure and pressure gradient. The scattered fields were obtained using the AEBEM2 subroutine of Kirkup (14), solving the Burton and Miller formulation for acoustic scattering. Figure 5 also shows results for the far-field directivity obtained using Curle's analogy (3). Curle's analogy is known to produce accurate results from incompressible flow field data when the geometry is acoustically compact, that is when $k_aD << 1$. The directivity of the scattered sound pressure is in very close agreement with the results obtained using Curle's analogy at the vortex shedding frequency. As the frequency increases, the acoustic compactness of the geometry decreases and hence an incompressible implementation of Curle's analogy becomes less applicable. The directivity pattern for the first four harmonics of the vortex shedding frequency is a dipole. The axis of the dipole is aligned perpendicular to the direction of fluid flow for the vortex shedding frequency and its third harmonic, corresponding to sound produced by the fluctuating lift force on the cylinder. For the second and fourth harmonics of the vortex shedding frequency, the dipole is oriented parallel to the direction of fluid motion, corresponding to sound produced by the fluctuating drag force on the cylinder. The directivity at all four frequencies predicted using Curle's analogy and the incompressible flow field data have a perfect dipolar shape. However the results obtained using the near-field formulation developed here become increasingly distorted as the frequency increases. This is due to the fact that the near-field formulation is able to include diffraction of the sound waves by a non-compact body.

3.2.2 Coupled near-field formulation and particle condensation technique

The scattered fields predicted using the coupled near-field formulation and particle condensation technique are presented and compared with the results obtained using only the near-field formulation. Figure 6 presents the scattered acoustic pressure at $r = 6000D$ for the first four harmonics of the vortex shedding frequency for window parameters $L_{w1} = 1.44d_1$ and $L_{w2} = 3.96d_1$. Figure 6 shows that the far-field scattered pressure obtained with the coupled near-field formulation and particle condensation technique matches well with the results obtained using only the near-field formulation. Using the coupled approach with zeroth moments of the acoustic sources used in the particle approximation (0MPC), the scattered acoustic pressure is predicted within 1% of the full near-field formulation solution at the fourth harmonic of the vortex shedding frequency, with reduction by a factor of 5 in the data storage and corresponding increase in acceleration of the acoustic propagation calculations. Significantly greater accuracy is achieved at lower frequencies. There is a slight discrepancy between condensed and non-condensed results at the fourth harmonic and this discrepancy becomes larger as the order of spatial condensation increases. The reason is that the higher order spatial condensations involve Green's function derivatives with higher order singularities. Hence, the proximity of the particles to the cylinder body results in a reduction in accuracy when evaluating the Green's function derivatives of the higher order condensations.

4. CONCLUSIONS

A particle accelerated CFD-BEM technique has been developed to predict the flow induced noise generated by a rigid body immersed in an unsteady flow. The method extracts the acoustic sources based on Lighthill's analogy from incompressible CFD data and computes the propagation of the resulting acoustic waves from the flow noise sources to the surface of the body. To calculate the incident acoustic field on the body, the domain is split into two regions. The inner region, which contains the body, is solved using formulations for the near-field pressure and pressure gradient based on Lighthill's analogy. The outer region is solved using a particle condensation technique for the near-field pressure and pressure gradient. Hence, the near-field effects are accurately resolved. Further away from the body, the acoustic sources are spatially condensed to reduce the amount of data that must be stored and accelerate the acoustic propagation calculations. The incident field on the body calculated using the coupled near-field formulation and particle condensation technique is then applied to an existing BEM solver based on the Burton and Miller formulation to predict the radiated sound pressure. This particle accelerated CFD-BEM technique has been applied to predict the scattering of sound waves produced by laminar vortex shedding from a two-dimensional cylinder at a Reynolds number, $Re_D = 100$ and Mach number, $M = 0.02$. The scattered far-field sound pressure predicted with the present method compares well with results obtained using Curle's analogy when the body is acoustically compact. Using the coupled approach, the scattered acoustic pressure is predicted within 1% of the full near-field formulation solution at the fourth harmonic of the vortex shedding frequency, with reduction by a factor of 5 in the data storage and corresponding increase in acceleration of the acoustic propagation calculations. Significantly greater accuracy is achieved at lower frequencies.

REFERENCES

1. Lighthill MJ. On sound generated aerodynamically, I. General theory. Proc Roy Soc A. 1952;211:564–587.

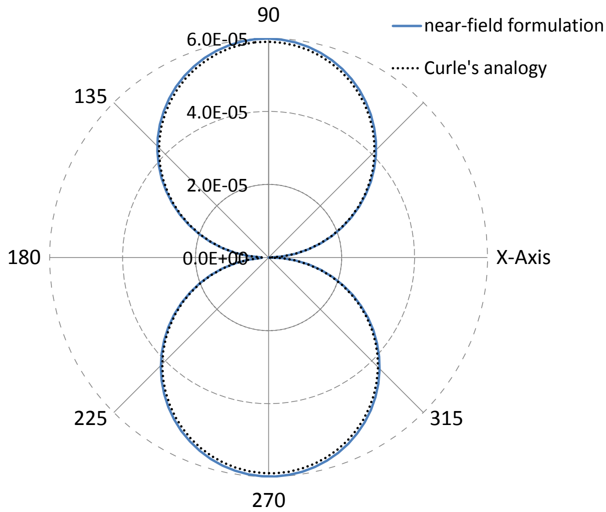

(a) Vortex shedding frequency

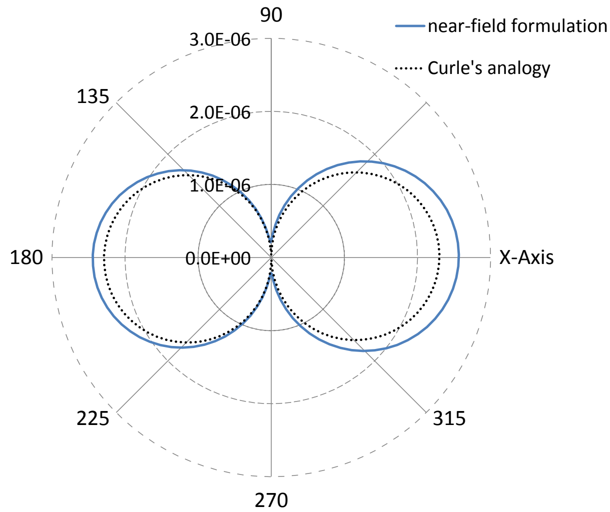

(b) Second harmonic frequency

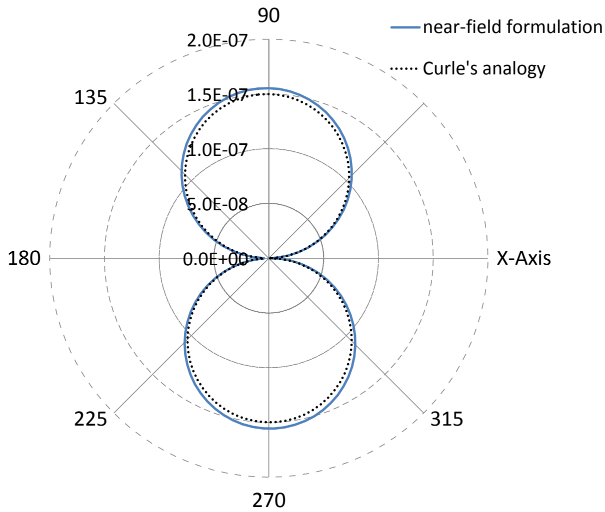

(c) Third harmonic frequency

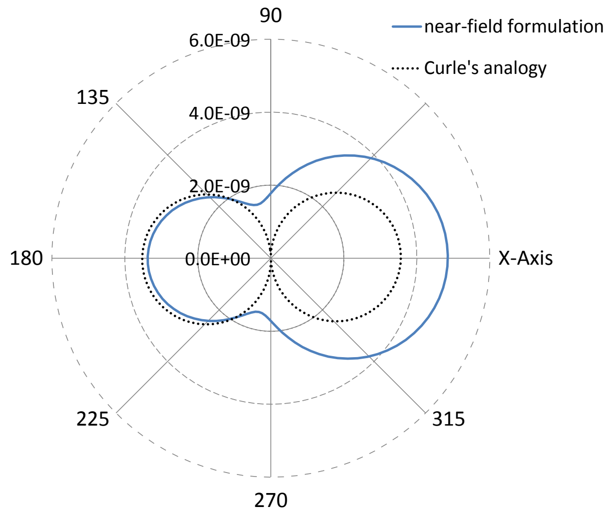

(d) Fourth harmonic frequency

Figure 5 – Directivity of the scattered acoustic pressure normalised by $\rho_0 U_\infty^2$, at $r = 6000D$ for the first four harmonics of the vortex shedding frequency, showing results computed using the near-field formulation and results using Curle's analogy

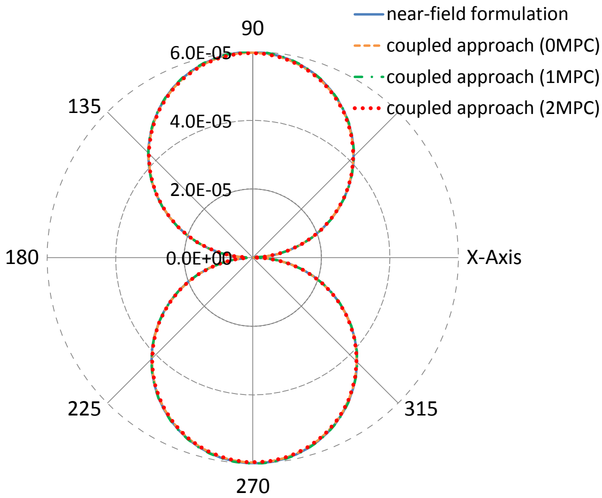

(a) Vortex shedding frequency

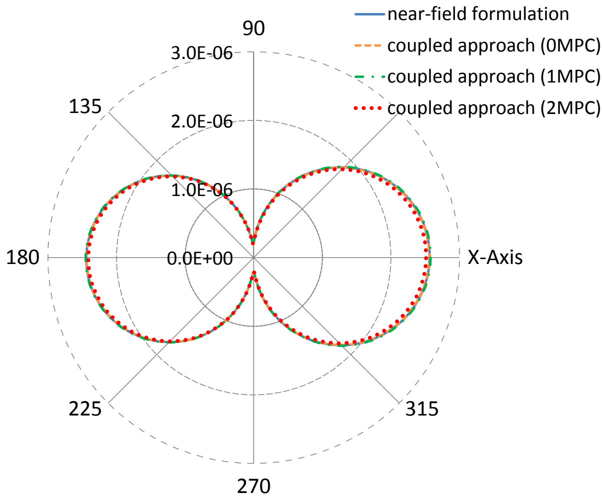

(b) Second harmonic frequency

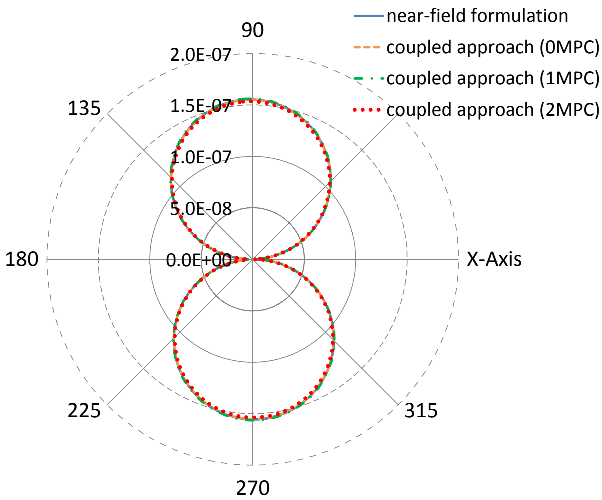

(c) Third harmonic frequency

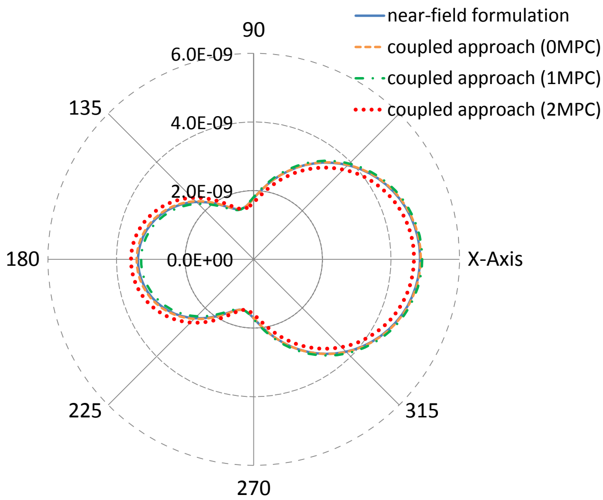

(d) Fourth harmonic frequency

Figure 6 – Directivity of the scattered acoustic pressure, normalised by $\rho_0 U_\infty^2$, at $r = 6000D$ for the first four harmonics of the vortex shedding frequency, showing results computed using only the near-field formulation, and results with the coupled near-field formulation and particle condensation (mMPC) technique

2. Lighthill MJ. On sound generated aerodynamically, II. Turbulence as a source of sound. Proc Roy Soc A. 1954;222:1–32.

3. Curle N. The influence of solid boundaries upon aerodynamic sound. Proc Roy Soc Lon A. 1955;231:505–514.

4. Gloerfelt X, Pérot F, Bailly C, Juvé D. Flow-induced cylinder noise formulated as a diffraction problem for low Mach numbers. J Sound Vib. 2005;287:129–151.

5. Schram C. A boundary element extension of Curle's analogy for non-compact geometries at low-Mach numbers. J Sound Vib. 2009;322:264–281.

6. Khalighi Y, Mani A, Ham F, Moin P. Prediction of sound generated by complex flows at low Mach numbers. AIAA J. 2010;48(2):306–316.

7. Khalighi Y. Computational Aeroacoustics of Complex Flows at Low Mach Number. Stanford University; 2010.

8. Schenk HA. Improved Integral Formulation for Acoustic Radiation Problems. J Acoust Soc Am. 1968;44:41–58.

9. Marburg S, Amini S. Cat's Eye Radiation with Boundary Elements: Comparative Study on Treatment. J Comput Acoust. 2005;13:21–45.

10. Burton AJ, Miller GF. The Application of Integral Equation Methods to the Numerical Solution of Some Exterior Boundary-Value Problems. Proc Roy Soc Lon A. 1971;323:201–210.

11. Martínez-Lera P, Schram C. Correction techniques for the truncation of the source field in acoustic analogies. J Acoust Soc Am. 2008;124:3421–3429.

12. Croaker P, Kessissoglou N, Marburg S. A CFD-BEM coupling technique for low Mach number flow induced noise. Proc Acoustics 2013; 17-20 November 2013; Victor Harbor, Australia, 2013.

13. Croaker P, Marburg S, Kinns R, Kessissoglou N. A fast low-storage method for evaluating Lighthill's volume quadrupoles. AIAA J. 2013;51:867–884.

14. Kirkup SM. The Boundary Element Method in Acoustics. Integrated Sound Software; 1998.

15. Fey U, König M, Eckelmann H. A new Strouhal–Reynolds-number relationship for the circular cylinder in the range $47 < Re < 2 \times 10^5$. Phys Fluids. 1998;10(7):1547–1549.

16. Norberg C. Flow around a circular cylinder: Aspects of fluctuating lift. J Fluid Struct. 2001;15:459–469.

17. Posdziech O, Grundmann R. A systematic approach to the numerical calculation of fundamental quantities of the two-dimensional flow over a circular cylinder. J Fluid Struct. 2007;23:479–499.